Field Investigation of the Effect of Operational Speed and Lateral Wheel Wander on Flexible Pavement Mechanistic Responses

Authors:

Mohammad Hossein Shafiee, M.Sc.
Ph.D. Candidate
Department of Civil & Environmental Engineering
University of Alberta
I. F. Morrison Structural Engineering Laboratory
9105 116 Street
Edmonton, AB T6G 2E9, Canada

Somayeh Nassiri, Ph.D., P.Eng.

Postdoctoral Fellow
Department of Civil & Environmental Engineering
University of Alberta
3-092 Markin/CNRL Natural Resources Engineering Facility
9105 116 Street
Edmonton, AB T6G 2W2
Office: 780-492-2867

Alireza Bayat, Ph.D., P.Eng. (corresponding author)
Assistant Professor
Department of Civil & Environmental Engineering
University of Alberta
3-092 Markin/CNRL Natural Resources Engineering Facility
9105 116 Street
Edmonton, AB T6G 2W2
Office: 780-492-5112
(Email) abayat@ualberta.ca

Abstract

Pavement design is evolving from the experimental American Association of State Highway and Transportation (AASHTO) Pavement Design Guide to the Mechanistic-Empirical Pavement Design Guide (MEPDG) (AASHTOWare Pavement ME Design). In the latter method, the predicted mechanistic responses of the pavement structure (strains and deflections) are empirically correlated to field-observed distresses. Therefore, mechanistic response data from instrumented, full-scale test road facilities are essential for the validation and further development of the MEPDG models. The University of Alberta's Integrated Road Research Facility (IRRF) includes an extensively instrumented test road, with a variety of asphalt strain gauges and earth pressure cells in the unbound layers to capture the flexible pavements' mechanistic responses to dynamic traffic loading.

This paper focuses on investigating the effect of operational speed and lateral wheel wander on longitudinal tensile and vertical compressive strain measurements at the bottom of the Hot Mix Asphalt (HMA) layer (ε_l and ε_c) and compressive stress measurements in the granular base course (GBC) and subgrade (σ_c). During a field experiment at the IRRF, a test truck with pre-determined axle loads was driven at four different speeds and two symmetric lateral offsets with respect to the outer wheelpath. Longer load durations (lower loading frequency) were observed at lower truck speeds in the HMA and unbound layers. Also, the magnitude of ε_l and ε_c increased when speed decreased. Similarly, higher vehicle speed resulted in less σ_c within the GBC and subgrade.

Sensitivity of fatigue cracking and rutting models in the MEPDG to operational speed was investigated in a sensitivity analysis. To do so, an MEPDG-simulation of the test section was developed using the backcalculated moduli of each layer obtained from Falling Weight Deflectometer (FWD) test performed at the IRRF. The rate of both alligator cracking and rutting was found to decrease at operational speed of 60 km/hr. It was also found that the MEPDG underestimates the effect of speed on the predicted fatigue cracking and rutting.

1. Introduction

1.1. Background

Pavement design is evolving from the traditionally used empirical American Association of State Highway Transportation Officials (AASHTO) Pavement Design Guide to the Mechanistic-Empirical Pavement Design Guide (MEPDG), which is also known as the AASHTOWare Pavement ME Design. This new Design Guide relies on critical pavement structural responses predicted based on the multi-layer linear-elastic theory. These structural responses include axial tensile strains at the bottom of the Hot Mix Asphalt (HMA) layer to predict bottom-up fatigue cracking, resilient vertical strains within the HMA layer to predict HMA rutting as well as vertical strains in the unbound layers to predict rutting in base/subbase and subgrade. The predicted structural responses are used to calculate the damage in the pavement over increments of time. The cumulative damage at the end of each time period is converted into commonly occurring distresses such as fatigue cracking and rutting through empirical transfer functions.

Prediction of structural responses, especially for flexible pavements, is a challenging task due to the viscoelastic properties of the HMA layer. Frequency of loading as a result of operational speed influences the amount of induced strain in the pavement. The influence of viscoelasticity of the HMA is currently incorporated in the MEPDG internal analysis through the construction of a theoretical master curve at hierarchal input Level 3. Depending on the user-defined operational speed and the HMA layer temperature during each increment of time, the proper complex dynamic modulus (E^*) is retrieved internally from the constructed master curve and is used in the multi-layer elastic theory to predict the pavement responses. Additionally, the predicted distress can also be influenced by lateral wander of traffic, which reduces the load concentration on the wheel path, resulting in lower induced strains and thereby distresses. Currently, the lateral wheel wander is assumed to follow a normal distribution pattern in the MEPDG, with the width (standard deviation) being a user-defined parameter[1]. It is imperative that the accuracy of the MEPDG predictions for pavement structural responses at different operational speeds, as well as wheel wander is validated with respect to field measurements.

1.2. Historical Review

1.2.1. Effect of operational speed on pavement responses

A number of past studies have focused on the effect of operational speed on a few structural responses of flexible pavements. At Pennsylvania State (Penn State) University test track, instrumented flexible pavement sections were subjected to controlled truck traffic at three speeds of 32, 56 and 80 km/hr [2]. The effect of speed on the longitudinal tensile strain at the bottom of the HMA layer (ε_l) was investigated in the Penn State study, while a Weigh-In-Motion (WIM) system was used to measure the dynamic weight of the truck at each speed. Strain measurements using H-type Asphalt Strain Gauges (ASG) showed that at lower speeds, the HMA layer experiences higher ε_l. Longitudinal tensile strain increased by a maximum of 50 percent when driving at 32 km/hr (tandem axle load measured at 77 kN) compared to speed of 56 km/hr (tandem axle load of 81 kN). According to the Penn State study, the influence of speed on ε_l was more pronounced when the test truck was empty than when the same truck was fully loaded [2].

In another study at the Centre for Pavement and Transportation Technology (CPATT) Test Road in Waterloo, Ontario, the impact of speed (also) on ε_l was investigated by conducting controlled vehicle tests at 5, 25 and 40 km/hr for a wheel load of 49 kN [2]. The CPATT study showed that ε_l increased by nearly 200 microstrains, when truck speed decreased from 40 to 5 km/hr. Measurements of compressive stress (σ_c) in the granular base layer at three speeds of 5, 25 and 40 km/hr resulted in different loading frequencies of 0.7, 3.5 and 5.5 Hz, correspondingly [3]. Another study conducted at Virginia Smart Road focused on investigating the impact of speed on σ_c. Earth Pressure Cells (EPC)s installed at five different depths in the HMA, granular and subgrade layers were used to measure σ_c at truck speeds of 10, 25, 40 and 70 km/hr. It was found that that σ_c pulse shape and thereby frequency of loading is a function of the depth below the pavement surface and vehicle speed. Results from the study's stress measurements showed that depending on truck speed, residual σ_c remained in the unbound layer for up to 0.5 sec at 9 km/hr in the pulse's unloading phase. The residual σ_c was greater at lower speeds [4].

1.2.2. Effect of wheel wander on pavement responses

At the National Center for Asphalt Technology (NCAT) test track located in Auburn, Alabama, wheel wander was accurately measured using a system of axle sensing strips [4]. Measurements were taken to characterize the wheel wander pattern on the test road and establish their impact on the pavement in-situ measured responses. As shown in Figure 1, a strong relationship, in the form of a second-order polynomial function, exists between wheel wander and ε_l.

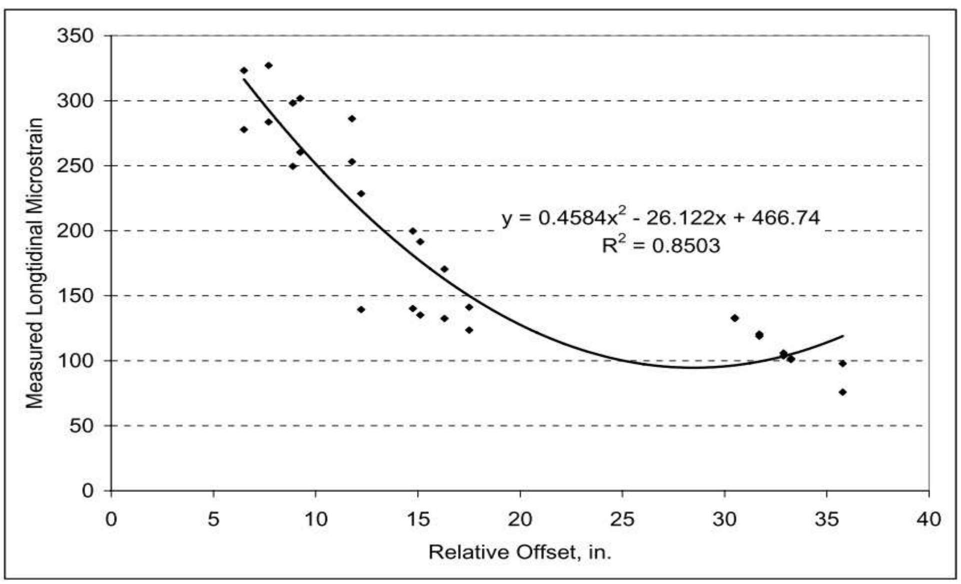

Figure 1- Effect of lateral wheel wander on ε_l (after [4]).

The change in wheel location from a zero-offset to a 30-inch offset relative to the centre of the ASG can drastically reduce ε_l from 300 to 100 microstarin in some cases [5]. Lateral wander of traffic is identified in the MEPDG documentation as a significant factor in the prediction of major pavement distresses, i.e. fatigue cracking and rutting, as variation can influence the number of axle load applications at a point of interest for performance prediction [6].

1.3. Scope of Work and Objectives

The literature review provided in the previous section revealed that operational speed and lateral wheel wander from the wheel path are influential on flexible pavement responses. However, the number of test runs included in each experiment is limited and the range of parameters, such as speed and wheel wander, requires expansion. Furthermore, the few studies reviewed above focused on quantifying the impact of speed on ε_l, which is the critical response in predicting fatigue cracking. However, the impact of speed on vertical compressive strain at the bottom of the HMA layer (ε_c), which is the primary response in predicting HMA rutting has not been investigated in the field. A similar drawback also applies to the studies conducted on the impact of wheel wander on the in-situ responses with primarily focus on on ε_l.

The current paper will present the result of a field experiment conducted on the University of Alberta’s Integrated Road Research Facility (IRRF)’s test road. the objectives of this paper are to investigate the impacts of vehicle’s operational speed and wheel wander on ε_l and ε_c at the bottom of the HMA. In addition, the effect of wheel wander on the measured σ_c at different depths in the unbound layers will be investigated.

The road’s extensive instrumentation enables simultaneous measurements of a variety of pavement responses under traffic loading including ε_l, ε_c and σ_c. A controlled truck loading test was conducted at the facility at three different speeds to fully investigate the effect of speed on in-situ measured critical responses. Furthermore, to address the need to assess the variation of induced responses against different wheel wanders, test runs at two offsets were conducted at the test road. Finally, this paper will investigate the extent of the effect of varying operational speeds on the MEPDG-predicted fatigue cracking and rutting.

2. Overview of Experiment

2.1. IRRF Test Road Facility

The IRRF’s test road facility is the new access road to Edmonton Waste Management Centre (EWMC) located Northeast of Edmonton, Alberta. Once opened to traffic (tentatively in summer 2015), the test road will be subjected to more than 500 garbage trucks per day transporting waste materials to EWMC. The test road comprises two approximately 100-m apart pavement monitoring sections (Sections 1 and 2). The pavement structure at Sections 1 and 2 is composed of a 250-mm HMA layer, placed atop a 450-mm granular base course (GBC) over clayey-sand (SC) subgrade soil.

2.2. Instrumentation Layout

During the construction of the test road in summer 2012, the test sections were instrumented with ASGs (Model CEA-06-125UT-350 from the CTL Group) and EPCs (Model LPTPC12-S from rst instruments) in the unbound layers. High-speed CR9000X datalogger from Campbell Scientific Corp Canada is used to collect the dynamic response of both sections at 500 Hz under moving trucks. Both sections are similarly instrumented at the bottom of the HMA layer with six

ASG laid in the longitudinal direction (ASG-L), six ASG laid in the transverse direction (ASG-T) and six vertical ASG (ASG-V). Figure 2 (a) shows the instrumentation layout, which is replicated in Sections 1 and 2 at the IRRF's test road. As shown in Figure 2 (a), the ASGs are arranged in three lines, where the middle array of gages is located on the outer wheelpath (OWP) and includes two ASG-V at the two outer ends, two ASG-L, each 600 mm to the inside of the ASG-V and 600 mm apart, and two ASG-T each laid at 600 mm distance from their corresponding ASG-L. To ensure of repeatability of the measurements and to provide for redundancy, the arrangement of the ASGs along the OWP was replicated in two additional lines, 600 mm to the right and 600 mm to the left of the OWP. EPCs were also installed at two locations, on the OWP and another one on the inner wheelpath (IWP). As seen in Figure 2 (b) each location includes three EPCs installed at three different depths. EPC 1 and 2 were installed at 100 mm from the top of the GBC; EPC 3 and 4 were installed at the top of the subgrade, and EPC 5 and 6 were installed at 1,000 mm from the top of the subgrade layer to monitor the distribution of load in the pavement underlayers.

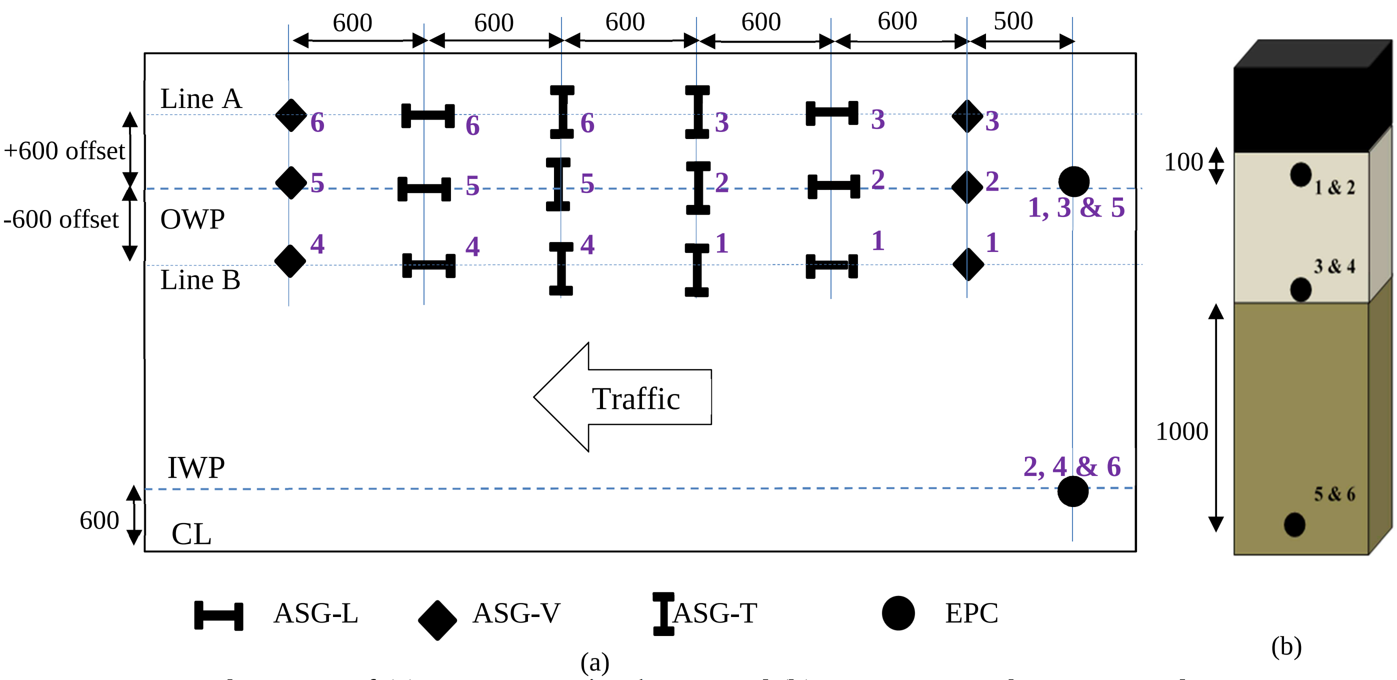

Figure 2- Schematics of (a) instrumentation layout and (b) cross section showing EPC locations for Sections 1 & 2 (all dimensions are in mm).

2.3. Controlled Vehicle Testing

As shown in Figure 3, a controlled vehicle testing was conducted at the IRRF' test road facility on July 25, 2013 using a two-axle, six-tire single unit truck with steering axle width and dual tire spacing of 1,700 mm and 2,000 mm, respectively and axle spacing (wheelbase) of 4,500 mm. Tires inflation pressure was 550 kPa. The rear axle was loaded to 3,000 kg and the steering axle weighed 1,530 kg. The first round of test runs were conducted at Section 1 at around noon, followed by the second round of tests conducted at Section 2 in the afternoon. The HMA temperature was measured at 20 mm below surface before each run. The average measured temperature in Sections 1 and 2 were 34 and 39°C. Four target speeds of 10, 20, 40 and 60 km/hr were included in the experiment. To investigate the effect of lateral wheel wander on the measured responses, tests were conducted along the OWP as well as along Lines A and B as shown in Figure 1, which are 600 mm to the right and 600 mm to the left of the OWP.

As seen in Figure 3, a second person assisted the driver in driving along the pre-determined lines by positioning the front wheel on the driver's side on: 1) Line A for +600 mm offset, 2) Line B -600 mm offset and 3) OWP line. The runs along each line were repeated at the four target speeds in three replicates, resulting in a total of 3×4×3 = 36 runs at each section. Videos were recorded from the road shoulder during each run to later check the wheelpath relative to gauge location for accuracy purposes.

In this study, strains from ASG-L and ASG-V located directly under the front wheel on the driver's side were considered for analysis. Strains from ASG-L #3 and #6, ASG-T #3 and #6 as well as ASG-V #3 and #6 were collected for the induced response from the truck when travelling along Line A. It is worth noting that ASG-V #6 in Section 1 in addition to ASG-V #5 and #6 in Section 2 were damaged during construction. Therefore, total of [4 speeds × 3 replicates × 5 gauges= 60] and [4 × 3 × 4 = 48] ε_c pulses were collected in Sections 1 and 2, respectively. Also, a total of, [4 × 3 × 6= 72] ε_l pulses was collected and analyzed in each Section. In addition, for all the cases stresses were obtained from EPC 1, and 3 in Section 1 and EPC 1, 3 and 5 in Section 2. Note that, EPC 5 installed at 1,000 mm in the subgrade in Section 1 was damaged during construction. Therefore, [36 × 2 = 72] σ_c pulses in Section 1 and [36 × 3 = 108] σ_c pulses in Section 2 were acquired for analysis.

Figure 3- Pre-loaded single unit truck used in the experiment.

3. Analysis of Collected Data

3.1. Impact of Operational Speed on Pavement Response

In order to investigate the effect of speed on the measured responses, i.e. ε_l, ε_c, and σ_c, truck loading was conducted along the OWP at different speeds. Since the test truck was not equipped with a cruise control, the actual speed differed from the target speed. To establish the actual speed, the duration between the two peak stresses corresponding to the steering and rear axles for each gauge and the truck wheelbase was used to calculate the actual speed. Figure 4 presents an example pulse measurement under both axles of the truck used for calculating operational speed.

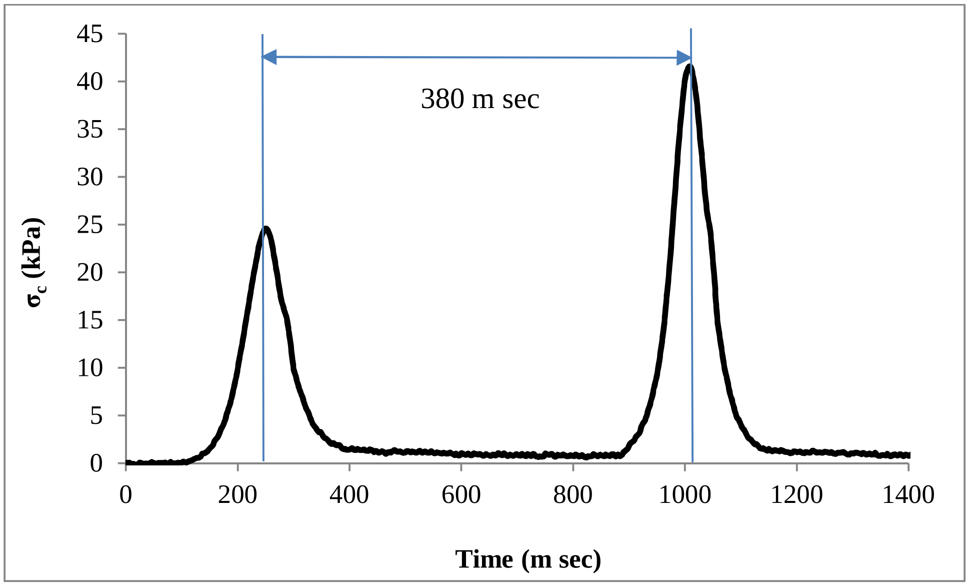

Figure 4- Example σ_c pulse under steering and rear axle loading.

Figure 5 shows an example σ_c from EPC 1 pulse measurement at 100 mm from the top of the GBC. The four pulses in the figure correspond to the four speeds when driving on top of EPC 1. In response to actual speeds of 20, 40 and 50 km/hr, peak σ_c levels of 25.5, 18.7 and 17.2 kPa were recorded at 100 mm in the GBC layer. Overall, compared to the stress measured at 10 km/hr, as speed increased to 20, 40, and 50km/hr, the recorded stress within the GBC showed 8, 48 and 84-percent decrease, respectively. The load pulse duration were 380, 256 and 128 and 84 msec for the 10, 20, 40 and 50 km/hr speeds, respectively, showing longer durations at lower speeds. Lower σ_c at higher speeds can be attributed to the viscoelastic behavior of HMA when subjected to vehicle loading. HMA shows higher stiffness at higher loading frequencies resulting in lower amount of σ_c transferred to the GBC layer.

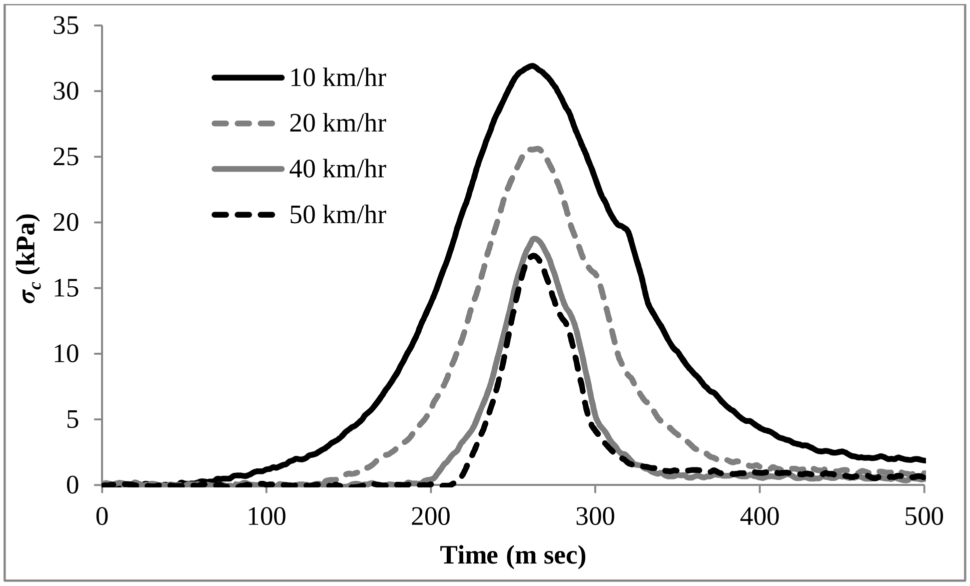

Figure 5- Example effect of actual speed on σ_c measured at 100-mm in the GBC in Section 1.

Similarly, an example of ε_l pulse measurements is provided in Figure 6 for the truck travelling on top of ASG-L #2 at the four different actual speeds. It is observed that the strain time histories followed a compression-tension-compression behavior for all the speeds. The four vehicle runs resulted in four symmetric pulse shapes with corresponding peak values of 77 to 66, 36 and 29 microstrain in tension. The duration of the strain pulse in tension also decreased at higher speeds (32, 76, 84 and 108 msec for the four speeds). The inverse of loading time provides the loading frequency, which were determined to be 31, 13, 12 and 9 Hz for actual speeds of 50 to 40, 20 and 10 km/hr, respectively. In addition, the magnitude of tensile portion of ε_l was determined as 77, 64, 36 and 29 microstrain when the truck speed decreased from 50 to 40, 20 and 10 km/hr, respectively. Additionally, the ratios between tensile to compressive strains were calculated equal to 2.6, 2.0, 2.0 and 2.2 for speeds of 10, 20, 40 and 50 km/hr, respectively.

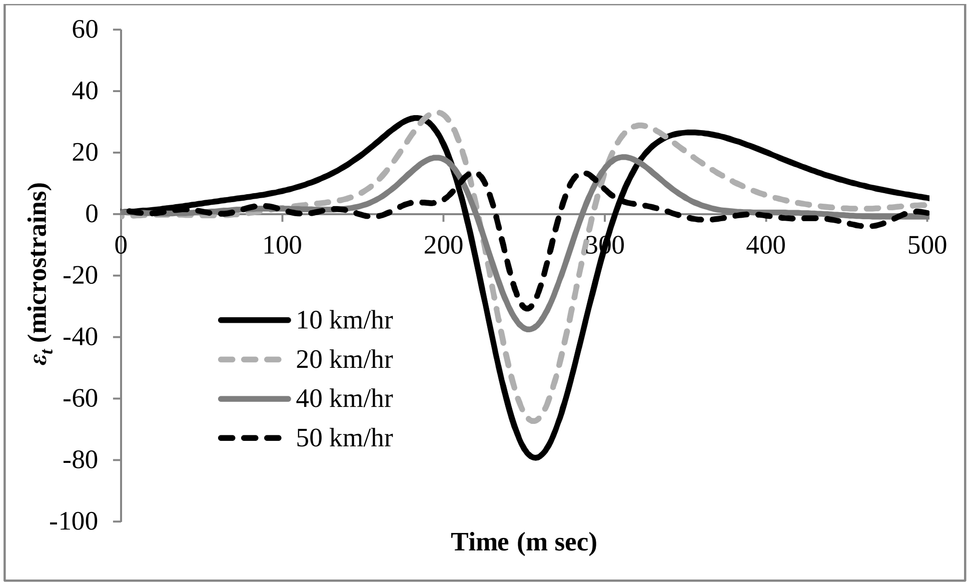

Figure 6- Example effect of speed on ε_l measured at bottom of HMA in Section 1.

In order to investigate the effect of speed on ε_c, this parameter was measured when the tire passed over ASG-V #2. Figure 7 confirms that the loading time, determined based on the first half of the pulse, is a function of speed. On the other hand, the pulse shape was noted to be symmetric at 50 km/hr, while the second half of the pulses were skewed to the right at 40, 20 and 10 km/hr speeds creating asymmetric pulses. According to Figure 7, under actual truck speeds of 50, 40, 20 and 10 km/hr, load durations were calculated to be 60, 136, 180 and 284 m sec, which correspond to 16.5, 7.5, 5.5 and 3.5 Hz. Values of ε_c were measured as 98, 200, 385 and 705 microstrains at the four different speeds. As shown in Figure 7, the amount of residual ε_c under the single tire increased at lower speeds. This agrees with the findings of Loulizi et al. (2002) [3] who reported residual stresses in the unloading phase of the stress pulses at Virginia Smart Road test facility. The residuals were up to near 10 percent of stress pulse peak value and were function of truck speed and reduced at higher speeds. Also, the induced ε_c returns to its initial zero value in shorter time durations at higher speeds.

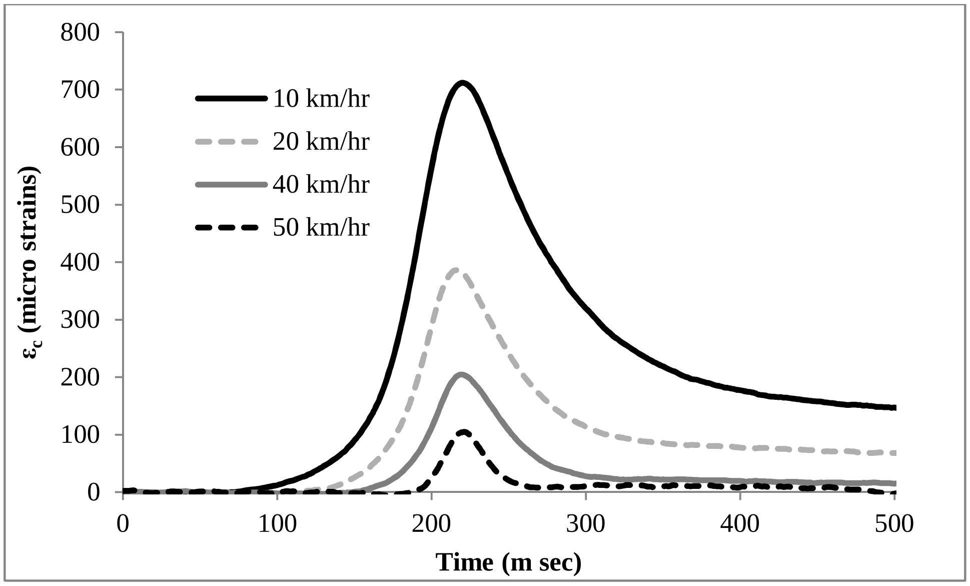

Figure 7- Example effect of speed on ε_c in Section 1.

3.2. Strain-Operational Speed Relationship

In order to establish a relationship between the measured ε_l and speed all the peak strain values for the zero-offset runs were plotted against their corresponding actual truck speed. Figure 8 (a) and (b) depict the effect of varying speeds on measured ε_l for all of the collected data in Sections 1 and 2, respectively. It is noteworthy that the HMA temperature changed by 3 and 2°C during the runs at Section 1 and Section 2, respectively and therefore the temperature is believed to have had a negligible impact on ε_l values.

According to Figure 8 (a) and (b), a difference of 50 microstrains (60 percent reduction) was calculated between ε_l at minimum and maximum test speeds in Section 1, while this reduction was 43 microstrains (40 percent) in Section 2. The descending trend between ε_l and speed was more pronounced in Section 1 compared to Section 2.It is worth mentioning that accurate positioning of the truck wheels along the marked lines on the pavement was a challenge and varied between the two sections. . Overall, steering the truck along the lines was a challenging task and the Standard Error of the Estimate (SEE) of the relationships derived in Figure 8 (a) and (b) can be substantially reduced by using traffic delineation devices to reduce the wheel wander.

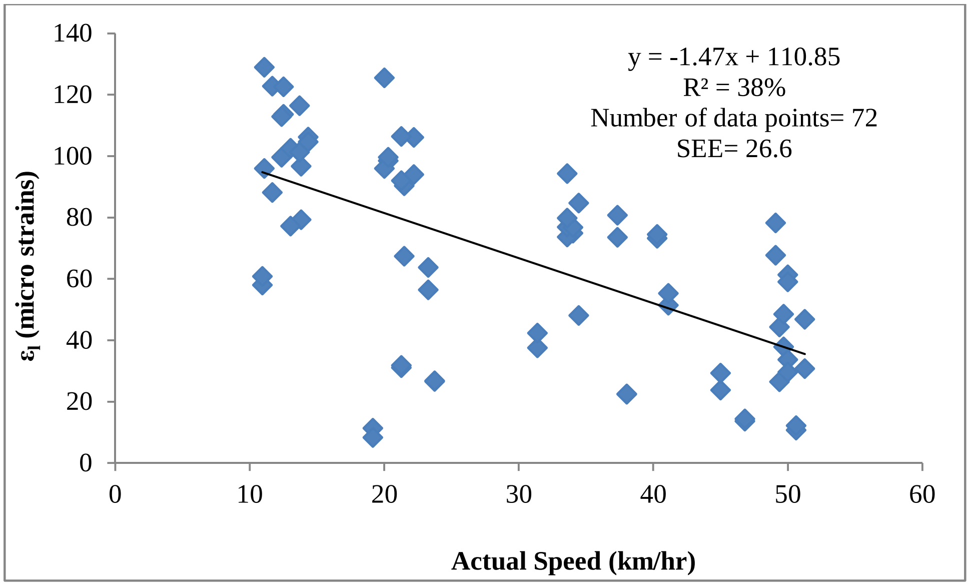

(a)

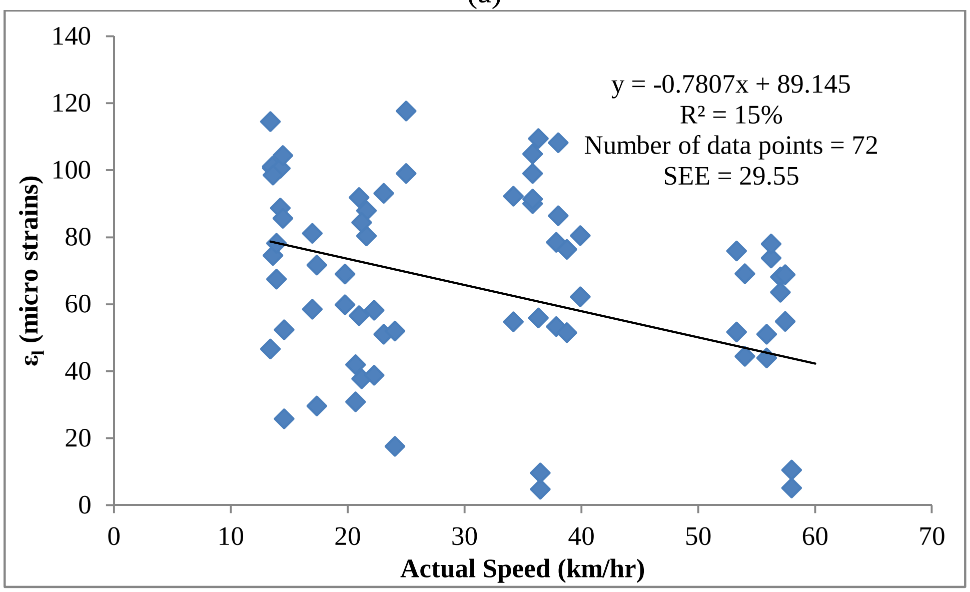

(b)

Figure 8- Variation of ε_l against truck speed for (a) Section 1 and (b) Section 2.

Similarly, all of the peak ε_c measured in Sections 1 and 2 at zero-offset were plotted against different speeds and are shown in Figure 9 (a) and (b), respectively. As illustrated in Figure 9 (a) and (b), ε_c generally decreased at higher speeds, implying less HMA rutting resistance at lower speeds. A reduction of 655 microstarins (87 percent) was noted between the recorded ε_c when increasing the speed from 10 and 55 km/hr in Section 1. Figure 9 (b) shows that this reduction is 995 (60 percent) for the range of variation in speed.

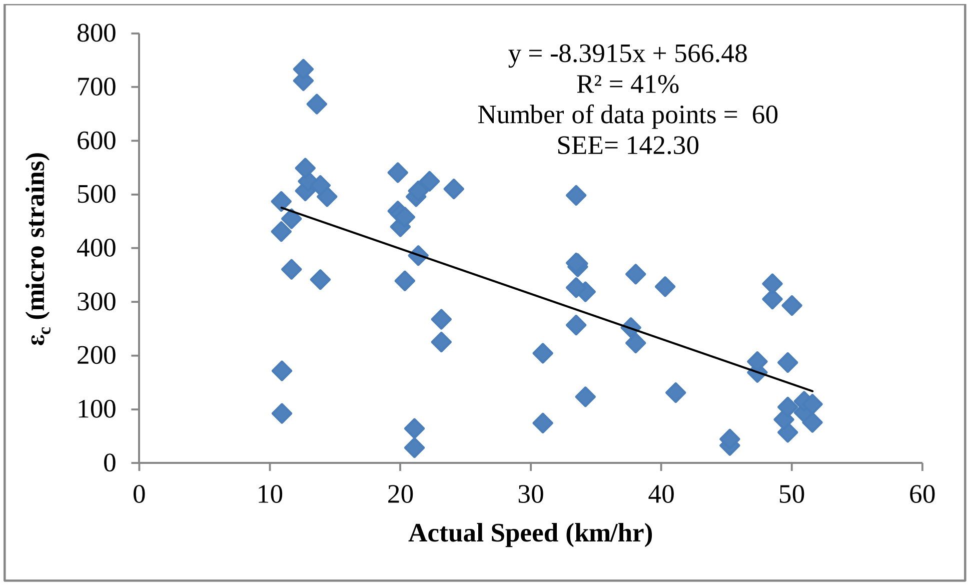

(a)

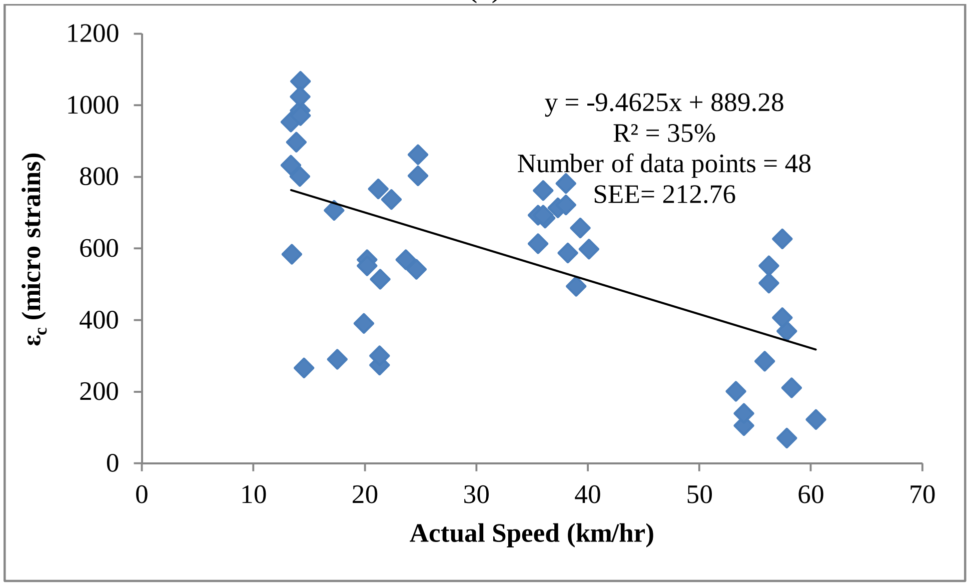

(b)

Figure 9- Variation of ε_c against speed in (a) Section 1 and (b) Section 2.

3.3. Impact of Wheel Wander on Pavement Response

An example of the impact of wheel wander on in-situ σ_c on top of the subgrade is shown in Figure 10from EPC 3 when subjected to truck speed of 10 km/hr. It should be noted that the truck load was not sufficient to study the effect of wheel wander on strain and therefore the impact of wheel wander was negligible on strain. As a result +600 mm and -600 mm offsets from the OWP led to almost zero microstrains at gauge locations, hence only the variation in σ_c against wheel wander is analyzed in this paper. Figure 10 depicts σ_c when the single tire on the steering axle was along Line A (+600 mm offset), OWP (no offset) and Line B (-600 mm offset).

Hence, the peak σ_c was measured equal to 7.2 kPa when the tire was positioned along OWP. However, the recorded σ_c decreased to 2.2 and 3.0 kPa as the position of the tire with respect to EPC 3 location increased to +600 mm and -600 mm from the OWP, respectively. It is noticed that the three pulses are almost symmetric in shape with identical loading frequencies associated with the first half of the pulses (1 Hz). The result of the test at zero offset relative to EPC 3 showed up to 0.5 kPa residual σ_c after the 1200 msec point, while the other two stress pulses recovered quickly after the steering axle pass.

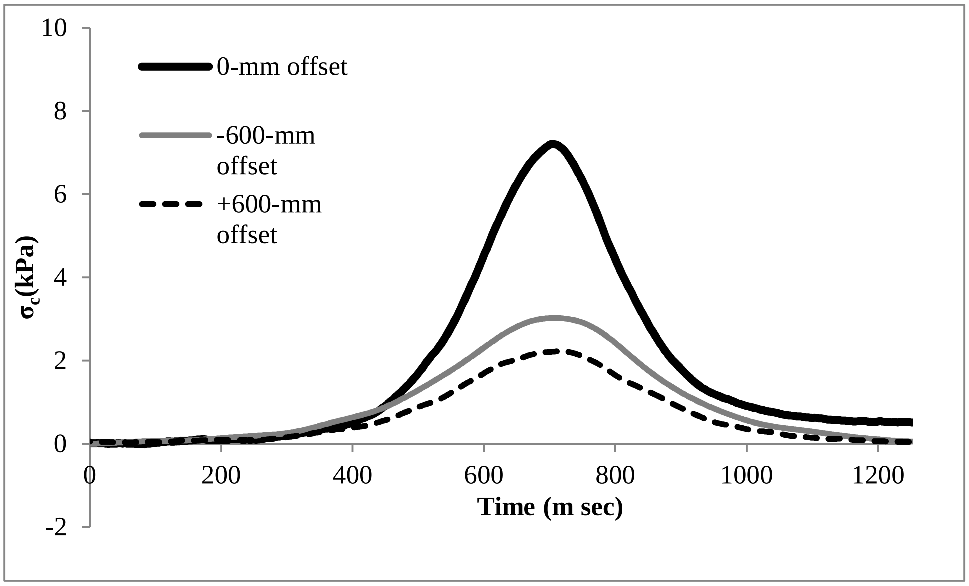

Figure 10- Effect of lateral wheel wander on σ_c at the top of subgrade in Section 1.

The distribution of σ_c within the GBC and subgrade can be investigated when the single tire on the steering axle passed over EPC 1, EPC 3 and EPC 5 location. Figure 11 presents a comparison between the three measured σ_c when the truck traveled at 10 km/hr along the OWP. Based on Figure 11, the shape of the measured pulse was found to be more elongated at 1000-mm within the subgrade (EPC 5) comparing to those recorded at top of the subgrade (EPC 3) and 100-mm within the GBC (EPC 1). Pulse duration at EPC 5 was 836 m sec, whereas pulse durations of 672 and 420 m sec were obtained at EPC 3 and 1 locations. The recorded load durations correspond to frequencies of 1.2, 1.5 and 2.4 Hz for EPC 1, EPC 2 and EPC 3, respectively. Figure 6 also demonstrates a significant decrease in the peak stress at deeper elevations indicating that σ_c reduced from 19.2 to 3.4 and 1.2 kPa at EPC 1, 3 and 5, respectively.

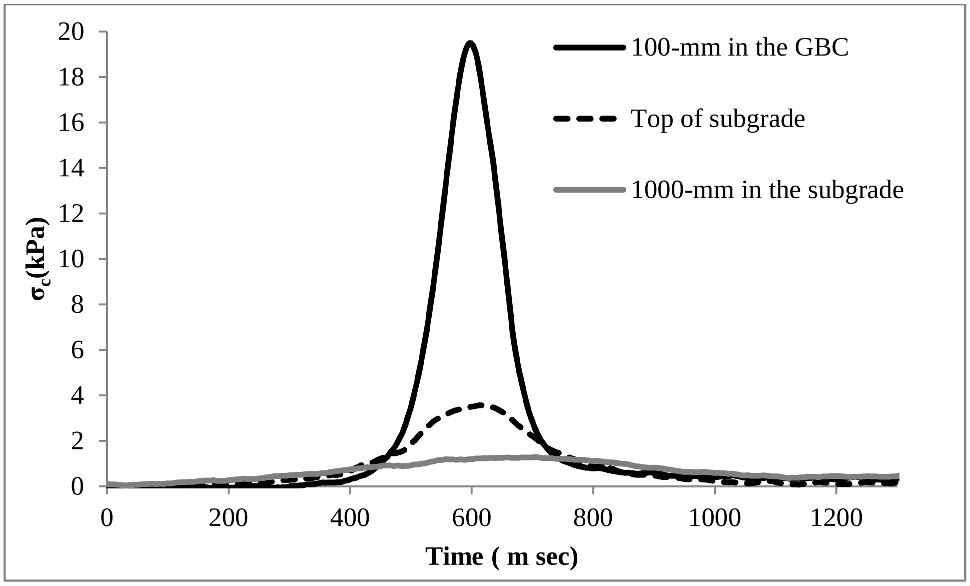

Figure 11- Example σ_c measured at different depths in unbound layers at 10 km/hr in Section 2.

3.4. Effect of Wheel Wander on Pavement Response

The impact of wheel wander on σ_c at 100-mm below GBC and also top of subgrade soil was examined for different speeds by using the OWP as the zero offset line and Lines A and B as +600-mm and -600-mm offsets relative to the OWP. Based on the results obtained for Section 1 (Figure 12 [a] and [b]), the recorded σ_c at 100-mm below GBC and top of the subgrade soil were the highest at zero offset. Further, the positive impact of speed on reducing σ_c was notable at three tested wheel wanders. According to Figure 12, the impact of wheel wander on σ_c was more distinct for the values at 100-mm in the GBC compared to the values recorded on top of the subgrade. Furthermore, testing at zero-offset led to a stronger σ_c–speed relationship than the passes at ±600-mm offsets.

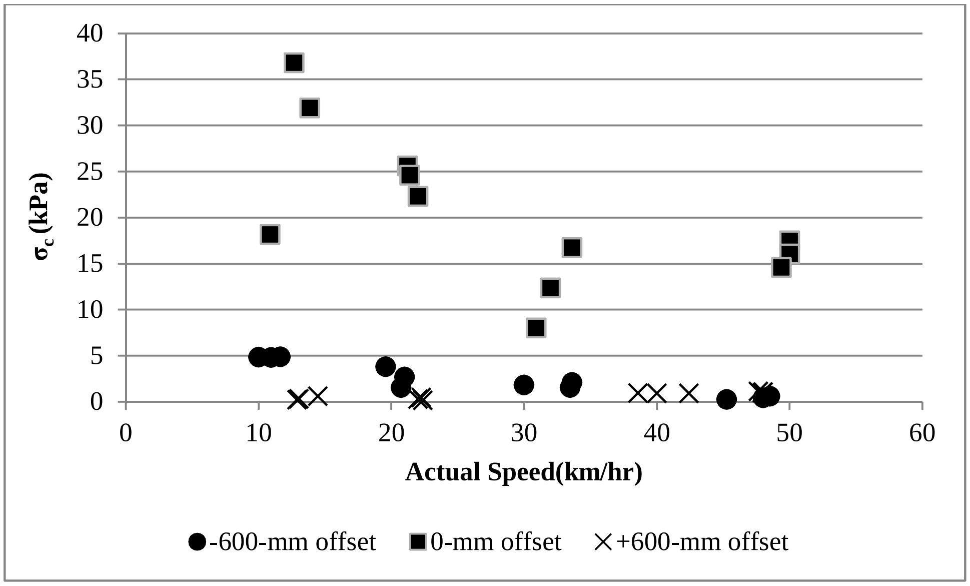

(a)

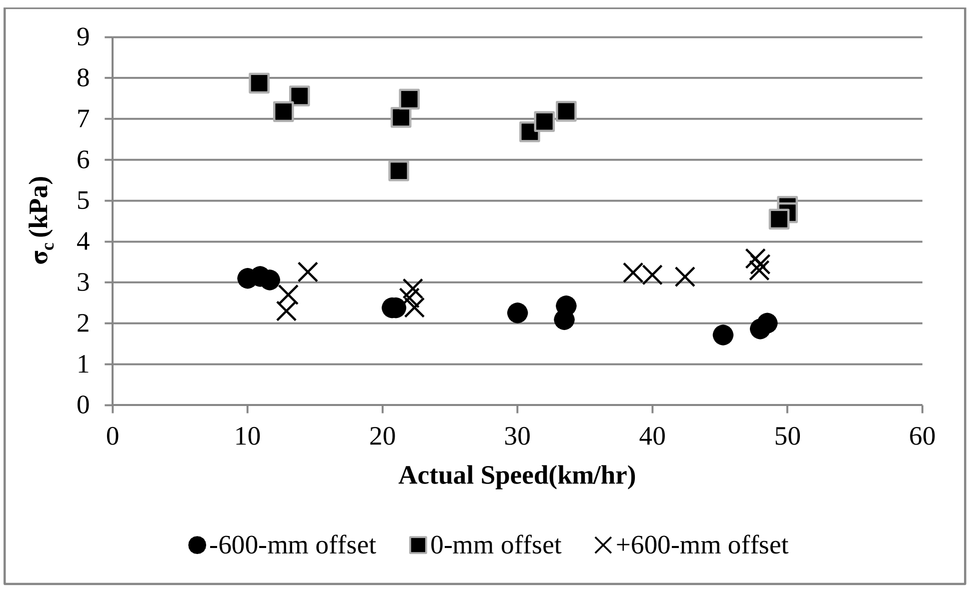

(b)

Figure 12- Variation of σ_c at (a) 100-mm in the GBC and (b) on top of the subgrade against wheel wander at different speeds in Section 1.

Similarly, Figure 13 (a) and (b) show the effect of wheel wander on σ_c at 100-mm in the GBC and top of the Subgrade layer based on the results in Section 2 when tested in similar pattern as Section 1. According to Figure 13 (a), the impact of wheel wander on σ_c was more distinct for the values at 100-mm in the GBC rather than the values recorded on top of subgrade. Furthermore, testing at zero-offset led to a stronger σ_c–speed relationship than the passes at ±600-mm offsets.

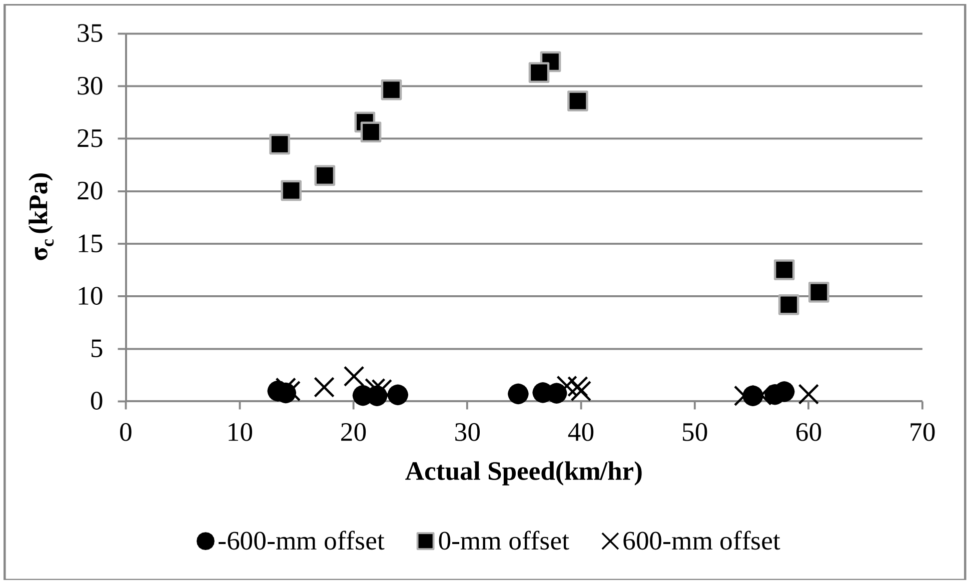

(a)

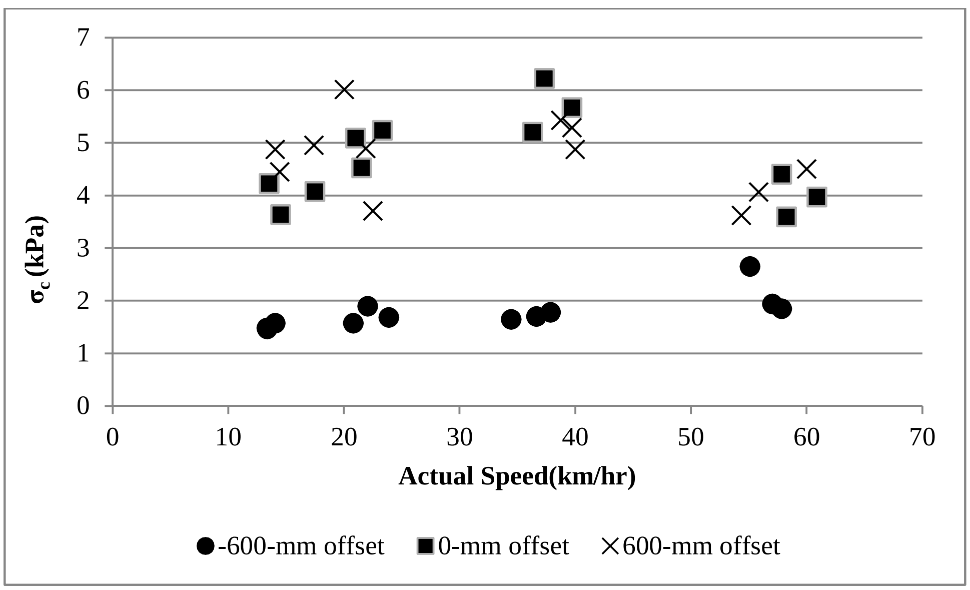

(b)

Figure 13- Variation of σ_c at (a) 100-mm in the GBC and (b) on top of the subgrade against wheel wander at different speeds in Section 2.

4. MEPDG Performance Prediction

4.1. Sensitivity Analysis

In the MEPDG, pavement performance is predicted by relating the pavement responses to distresses based on the user-defined traffic, material, and climate inputs. Fatigue and rutting in the HMA layer are the major distresses in flexible pavements; these distresses are directly associated with axial tensile and vertical compressive strains at the bottom of the HMA [1]. As the aforementioned critical responses are significantly affected by the vehicle operational speed, it is necessary to evaluate the extent of variation in the predicted performance in a range of speed. The MEPDG (Version 1.1) was used to investigate the effect of speed on the predicted distresses for the tests road. An MEPDG mode l of the test road was developed, defining the traffic, climate, and materials properties at input Level 1 where ever possible.

4.1.1. Input parameters

To determine the required material inputs for performance prediction, deflection data from the Falling Weight Deflectometer (FWD) test conducted on July 30, 2013 was used to backcalculate each layer's moduli. FWD tests were performed using 300-mm diameter loading plate at three stress levels of 380, 560 and 730 kPa along Sections 1 and 2. EVERCALC, developed by Mahoney et al. in 1989 [6] was used to backcalculate the elastic modulus of HMA, GBC and SC subgrade (E_{HMA}, E_{GBC}, and E_{SC}). As shown in

Table 1, typical values recommended in ASTM D5858 [7] for seed moduli and Poisson's ratio were defined in EVERCALC for each of the three layers. The backcalculated layer moduli are provided for Sections 1 and 2 in Table 1.

Table 1- Summary of backcalculation results for performance analysis.

Layer	Seed modulus (MPa)	Poisson's ratio	Backcalculated modulus (MPa)	
			Section 1	Section 2
HMA	3,500	0.35	1,537	1,796
GBC	200	0.40	120	115
SC subgrade	50	0.40	71	85

Table 2 summarizes the values used to define the input parameters at Level 1. The average backcalculated moduli for the subgrade and base from dynamic FWD testing need to be adjusted to agree with AASHTO resilient modulus test [8]. Alberta Transportation recommends multiplying the backcalculated moduli by a factor of 0.36 before using those values for design [9].Values for the other input parameters were kept as default. Total of 22 cases (11 operational speeds and two test sections) were modeled using the MEPDG and the 20-year predicted alligator cracking and HMA rutting are compared in Figure 14 and Figure 15.

Table 2- Summary of input parameters used in the MEPDG.

Group	Design parameter			Values	Comments
General	Design life (years)			20	
Traffic	Initial two-way AADTT			2,000	Based on traffic data from the EWMC
	Number of lanes in design direction			2	
	Percent of trucks in design direction (%)			50	
	Percent of trucks in design lane (%)			100	
	Operational Speed (km/h)			Varying from 10 to 110 km/hr	
Climate	Edmonton International Airport climatic file				Closest weather database available in the MEPDG. The database includes weather data from 7/1/1987 to 6/30/2007.
HMA	HMA Layer Thickness (mm)			250	Existing HMA thickness
	HMA Gradation		%Retained 3/4 in	0	Based on tests provided by the consultant
			%Retained 3/8 in	19	
			%Retained #4	36	
			%Passing #200	8.6	
	Binder Type		PG 58-28		
	Mixture properties		% Air voids	4	
			% Effective binder	9	
Unbound Materials	Base	Modulus	Section 1	43 MPa	Based on FWD tests on 30 July, 2013
			Section 2	41 MPa	
		Gradation	%Passing 3/4 in	99	Based on gradation analysis according to ASTM C 136-06 [10]
			%Passing 3/8 in	61	
			%Passing #4	42	
			%Passing #200	0.5	
	Subgrade	Modulus	Section 1	25 MPa	Based on FWD tests on 30 July, 2013
			Section 2	30 MPa	
		Gradation	%Passing #40	99	Based on gradation analysis according to ASTM C 136-06 [10]
			%Passing #100	84	
			%Passing #200	47	
Design Criteria	Terminal IRI		Distress target	2.74 m/km	MEPDG default values
	HMA surface-down cracking		Target	37,878.88 cm/km	
	HMA bottom-up cracking			25%	
	HMA thermal fracture			18,939.44 cm/km	
	Permanent deformation (HMA Only)			0.64 cm	
	Permanent deformation (Total pavement)			1.91 cm	
	Reliability			90%	

4.1.2. Performance predictions

According to Figure 14, 20-year predicted alligator cracking decreased in both sections as operational speed increased. The predicted alligator cracking and the corresponding reliability were approximately identical for both sections implying almost similar performance in Sections 1 and 2. It is observed that alligator cracking decreased approximately four percent when speed increased from 10 to 60 km/hr, however increasing speed by another 50 km/hr, from 60 up to 110 km/hr, resulted in only one percent reduction in the predicted distress. In other words, the reduction in fatigue cracking became less significant for speeds higher than 60 km/hr. Comparison between the four-percent performance improvement in fatigue life and the amount of reduction in ε_l (60 and 40 percent in Section 1 and 2, respectively) as a result of speed change from 10 to 60 km/hr indicates that perhaps the influence of speed is not truly reflected in the MEPDG design procedure. For speed range of 10 to 50 km/hr, predicted reliability failed the 90-percent default target, while speeds from 60 to 110 km/hr resulted in reliabilities of higher than 90 performance. All cases did meet the 25-percent of target for alligator cracking.

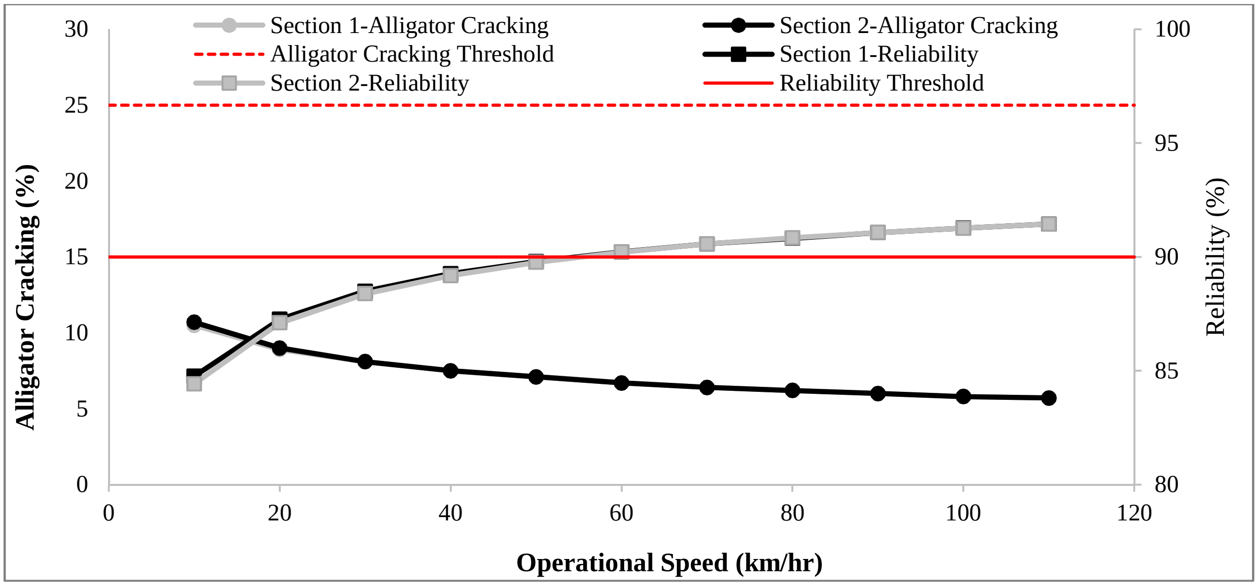

Figure 14- Comparison of alligator cracking at different speeds in Sections 1 and 2.

A similar analysis was performed to evaluate the impact of speed on the predicted HMA rutting. Figure 15 shows that the HMA rutting decreased as speed increased, which is attributed to smaller ε_c at higher speeds. According to Figure 15, while a 50-km/hr increase in speed (from 10 to 60 km/hr) leads to approximately six percent less HMA rutting, the same amount of increase from 60 to 110 km/hr causes 1.2 percent less HMA rutting. Hence, the rate of reduction in rutting depth is more pronounced at 10 to 60 km/hr speed range in comparison to 60 to 110 km/hr speed range. The six-percent less HMA rutting predicted using the MEPDG over the range of tested speeds in the field is not consistent with the actual change in the measured ε_c which varied nearly 87 and 60 percent as a result of the speed variation in Sections 1 and 2, respectively. This comparison shows that the effect of speed on the performance predictions in the MEPDG is not is not reflective of the field measured ε_c at the bottom of the HMA layer. All of the scenarios failed to meet the 90-percent reliability criteria; the best predicted reliability was limited to 45.2 percent at 110 km/hr speed. Furthermore, the criteria for maximum rutting depth in the analysis (64 mm) was not met for any of the scenarios; minimum rutting depth of 6.6 mm was predicted at 110 km/hr in Sections 1 and 2.

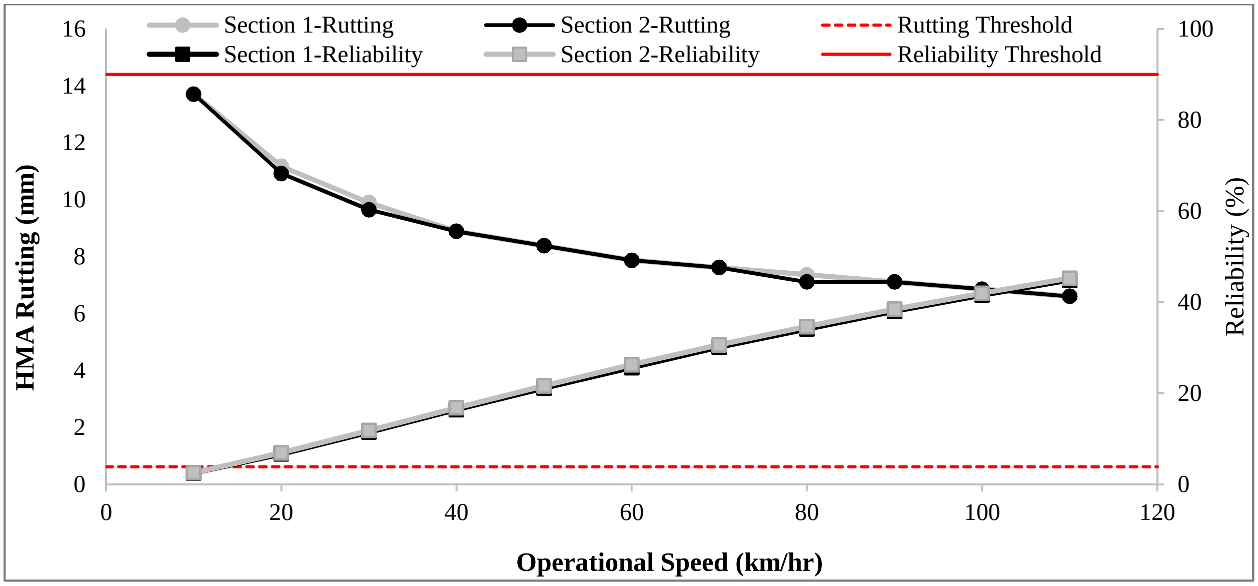

Figure 15- Comparison of HMA rutting at different speeds in Sections 1 and 2.

5. Conclusions

This study investigated the impact of operational speed and wheel wander on in-situ measured σ_c within the unbound layers, and ε_l and ε_c at the bottom of the HMA layer was conducted for two test sections at the IRRF's test road. Controlled vehicle testing was conducted using a pre-loaded single-unit truck at four operational speeds and two different offsets relative to the OWP.

Longer load durations (lower loading frequency) were captured at lower speeds by three types of gauges, EPCs, ASG-Ls and ASG-Vs. Additionally, ε_l and ε_c decreased up to 60 and87 percent in Sections 1 and 2, respectively, when speed increased over the tested range. Changing speed from 10 to 50 km/hr at zero offset relative to the EPCs location, σ_c within the GBC layer decreased up to 64, 48 in Sections 1 and 2, respectively. Residual stresses remained in the HMA layer at the end of the unloading phase, which decreased as speed increased. Evaluation of the impact of wheel wander on σ_c within the GBC and subgrade layers showed that ±600-mm offsets can significantly decrease the induced σ_c at 100-mm in the GBC and top of subgrade both sections. Maximum recorded σ_c at 100-mm in GBC reduced from 36.5 kPa at zero-offset to 5 kPa at -600-mm offset (86 percent reduction. Similarly, maximum value of σ_c on top of the subgrade was found equal to 8 kpa at zero-offset which reduced to 3 kPa at -600-mm offset (62 percent reduction).

In agreement with the field results which showed less critical ε_l and ε_c at higher speeds, the MEPDG-predicted distresses in both sections was lower at higher operational speeds. The rate in both alligator cracking and rutting was found to decrease at operational speed of 60 km/hr. The performance variation against speed using the MEPDG did not agree with the observed trend in ε_l and ε_c against speed. The observed field data showed larger variations in ε_l and ε_c versus speed which was not reflected well in MEPDG predictions.

Acknowledgements

The authors would like to acknowledge Alberta Transportation, Alberta recycling, and The City of Edmonton for providing financial and in-kind support for the construction and instrumentation of the IRRF's test road. Alberta Transportation is also acknowledged for sponsoring the Falling-Weight Deflectometer (FWD) tests for this study. Close cooperation of FWD test crews from EBA Engineering is also greatly appreciated.

References

[1] ARA, Inc., ERES Consultant Division. *Guide for Mechanistic–Empirical Design of New and Rehabilitated Pavement Structures*. Final report, NCHRP Project 1-37A. Transportation Research Board of the National Academies, Washington, D.C., 2004. http://www.trb.org/mepdg/guide.htm.

[2] P. E. Sebaaly and N. Tabatabaee, 1993. Influence of Vehicle Speed on Dynamic Loads and Pavement Response. In *Transportation Research Record: Journal of Transportation Research Board*, No. 1410, Transportation Research Board of the National Academies, Washington D.C., pp 107-114.

[3] A. Bayat, *Field and Numerical Investigation to Determine the Impact of Environmental and Wheel Loads on Flexible Pavement*. Doctoral dissertation, University of Waterloo, 2009.

[4] A. Loulizi, I. L. Al-qadi, S. Lahouar, and T. E. Freeman, 2002. Measurement of Vertical Compressive Stress Pulse in Flexible Pavements Representation for Dynamic Loading Tests. In *Transportation Research Record: Journal of Transportation Research Board*, No. 1816, Transportation Research Board of the National Academies, Washington D.C., pp 125-136.

[5] D. H. Timm and A. L. Priest, *Wheel Wander at the NCAT Test Track*, Report No 05-02, National Center for Asphalt Technology, Auburn University, Auburn, Ala., 2005.

[6] J. P., Mahoney, N. F., Coetzee, R. N., Stubstad, and S. W., Lee (1989). A performance comparison of selected backcalculation computer programs. *ASTM STP*, Vol. 1026, 452-467.

[7] ASTM D5858-96, Standard Guide for Calculating In Situ Equivalent Elastic Moduli of Pavement Materials Using Layered Elastic Theory, ASTM American Standard for Testing Materials, West Conshohocken, PA, 2008.

[8] *AASHTO Guide for Design of Pavement Structures 1993*. AASHTO, Washington, D.C., 1993.

[9] Alberta Transportation and Utilities, 1997. Pavement Design Manual, Edmonton, AB.

[10] ASTM C136-06, Standard Test Method for Sieve Analysis of Fine and Coarse Aggregates, ASTM American Standard for Testing Materials, West Conshohocken, PA, 2006.